Chemical Science

ROYAL SOCIETY OF CHEMISTRY

EDGE ARTICLE

View Article Online
View Journal | View Issue

Cite this: *Chem. Sci.*, 2023, **14**, 1472

All publication charges for this article have been paid for by the Royal Society of Chemistry

Fluorido-bridged robust metal–organic frameworks for efficient C_2H_2/CO_2 separation under moist conditions†

Yi-Ming Gu, [ab] You-You Yuan,[c] Cai-Lin Chen, [d] Sheng-Sheng Zhao, [a] Tian-Jun Sun, [a] Yu Han, [d] Xiao-Wei Liu, *[d] Zhiping Lai *[d] and Shu-Dong Wang *[a]

Received 5th December 2022
Accepted 2nd January 2023

DOI: 10.1039/d2sc06699h

rsc.li/chemical-science

The modern technology for acetylene production is inevitably accompanied by the contamination of carbon dioxide and moisture impurities. Metal–organic frameworks (MOFs), with rational configurations of fluorine as the hydrogen-bonding acceptor (HBA), exhibit excellent affinities to capture acetylene from the gas mixtures. Currently, most research studies feature anionic fluorine groups as structural pillars (*e.g.*, SiF_6^{2-}, TiF_6^{2-}, $NbOF_5^{2-}$), whereas *in situ* insertion of fluorine into metal clusters is rather challenging. Herein, we report a unique fluorine-bridged Fe-MOF, *i.e.*, DNL-9(Fe), which is assembled by mixed-valence $Fe^{II}Fe^{III}$ clusters and renewable organic ligands. The fluorine species in the coordination-saturated structure offer superior C_2H_2-favored adsorption sites facilitated by hydrogen bonding, with a lower C_2H_2 adsorption enthalpy than other reported HBA-MOFs, demonstrated by static/dynamic adsorption tests and theoretical calculations. Importantly, DNL-9(Fe) shows exceptional hydrochemical stability under aqueous, acidic, and basic conditions, and its intriguing performance for C_2H_2/CO_2 separation was even maintained at a high relative humidity of 90%.

Introduction

Acetylene (C_2H_2) is a vital building block for the synthesis of various chemical commodities. Its modern production methods, *e.g.*, pyrolysis, partial combustion, or thermal cracking of hydrocarbons, inevitably contaminate the product gas with carbon dioxide (CO_2) and moisture (H_2O).[1–3] These impurities pose a challenge in producing high-purity C_2H_2 in isolation for end-users, given the similarities in kinetic diameter (*i.e.*, 3.3 Å) and polarizability (*i.e.*, 33.3 *versus* 29.1 × 10^{25} cm^{-3}) between C_2H_2 and CO_2, along with the presence of vapor/moisture *via* physisorption-based pressure swing adsorption (PSA) and vacuum swing adsorption (VSA) processes.[4–7]

Metal–organic frameworks (MOFs) are promising sorbents for C_2H_2 separation owing to their tailorability in pores, surface chemistry and building units.[8–12] Particularly, the introduction of fluorine (F) into the backbone of MOFs is found to effectively enhance C_2H_2 adsorption, boost C_2H_2/CO_2 separation properties and the resistance to moisture, with fluorine species serving as the hydrogen bonding acceptor (HBA).[13–19] Two main strategies are reported to achieve the aim: (i) employing anionic fluorine groups, such as SiF_6^{2-}, TiF_6^{2-}, FeF_5^{2-} and $NbOF_5^{2-}$, to construct anion-pillared MOFs;[13–16] (ii) utilizing fluorinated organic linkers to form fluorine-containing MOFs like FMOF-1, FMOFCu and MOFF-5.[17–19] Although a few MOFs prepared by the above approaches have shown promise for C_2H_2/CO_2 separation, the fluorous reagents are relatively expensive. Also, most anion-pillared MOFs reveal high adsorption enthalpies for C_2H_2, *e.g.*, over 35 kJ mol^{-1}, which in turn, will cause an energy penalty during desorption. Besides, it is also fairly difficult to introduce highly coordinated fluorine moieties into MOFs, *e.g.*, the fluorination of metal nodes (Scheme 1).[20–22] The high ligancy of fluorine bonded with metal nodes as well as the hydrophobic micro environment, however, may protect the sites from being attacked by water molecules.[13]

We herein report a unique Fe-MOF, *i.e.*, DNL-9(Fe) (Dalian National Laboratory for Clean Energy, China), constructed from $Fe^{II}Fe^{III}$ clusters and biomass-derived 2,5-furandicarboxylic acid (FDCA) linkers. This material possesses a high coordination ligancy of bridged and terminal fluorine with metal nodes,

[a]*Dalian National Laboratory for Clean Energy, Dalian Institute of Chemical Physics, Chinese Academy of Sciences, Dalian, 116023, China. E-mail: wangsd@dicp.ac.cn*

[b]*University of Chinese Academy of Sciences, Beijing 100049, China*

[c]*Core Laboratory, King Abdullah University of Science and Technology (KAUST), Thuwal, 23955-6900, Saudi Arabia*

[d]*Advanced Membranes and Porous Materials Center, Division of Physical Sciences and Engineering, King Abdullah University of Science and Technology (KAUST), Thuwal, 23955-6900, Saudi Arabia. E-mail: zhiping.lai@kaust.edu.sa; xiaowei.liu@kaust.edu.sa*

† Electronic supplementary information (ESI) available: Full experimental details, characterization, additional adsorption measurement, theoretical calculations, supplementary summary. CCDC 2050430. For ESI and crystallographic data in CIF or other electronic format see DOI: https://doi.org/10.1039/d2sc06699h

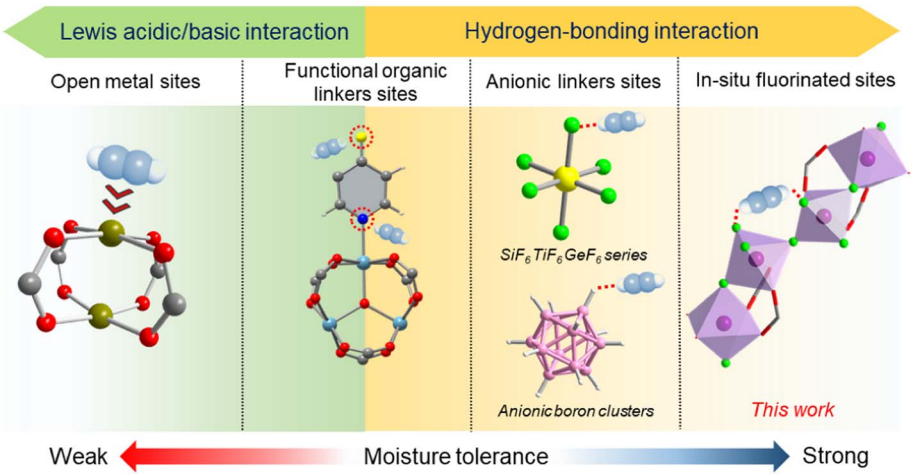

Scheme 1 Schematic showing state-of-art synthesis strategies for MOFs to achieve efficient C_2H_2/CO_2 separation. Gray, C; red, O; white: H; green, F; yellow: Si/Ti/Ge; pink: B; else: metal or functional group atoms.

which is very rarely reported in MOFs.[20,21,23] Hydrogen bonding could then be steadily formed between the framework and C_2H_2 molecules, *e.g.*, C–H···F and C–H···O_F (from furan rings), thus enhancing C_2H_2 capture. Consequently, these features endow DNL-9(Fe) with great potential to separate C_2H_2 from other gas impurities under moist conditions in the current production technology. The prominent C_2H_2/CO_2 performance of DNL-9(Fe) was then confirmed by a plethora of static/dynamic adsorption measurements and theoretical calculations. Furthermore, our work also demonstrated the exceptional hydrochemical stability of DNL-9(Fe) under aqueous, acidic, and basic conditions, and its excellent C_2H_2/CO_2 separation property was even maintained at a high relative humidity of 90%.

Results and discussion

To decode the fine structure of DNL-9(Fe), we obtained its single-crystal (Fig. S1†), and details of the crystallographic information are given in Table S1.† Also, the following X-ray fluorescence (XRF) measurement and elemental analysis determined the chemical composition of the structure, with calculated formula basically matching with that obtained from the single crystal (Table S2†). Fig. 1a and b illustrate the orthogonal structure of DNL-9(Fe) with a $P2_12_12_1$ space group, in which the chain-linked metal molecules precisely pack in an alternating helical pattern, and carboxylate groups of the FDCA ligands bridge helical $Fe_6(\mu\text{-}F)_6F_8$ clusters to ultimately form a chiral topology framework with pore channels running along different axes (Fig. 1c). There are two sets of μ-F and terminal F linkers that connect each hexa-coordinated Fe atom, *i.e.*, Fe–F–Fe and Fe–F; distinct from oxygen linkages, this is seldom explored in MOFs.[20,21,23] The saturated Fe units were divided into mixed-valence $Fe^{II}(\mu\text{-}O)_4\alpha\text{-}(\mu\text{-}F)_2$ and $Fe^{III}(\mu\text{-}O)_2\alpha\text{-}(\mu\text{-}F)\beta\text{-}(\mu\text{-}F)F_2$ characters, due to the reducing environment arising from the decomposition of *N*,*N*-dimethylformamide (DMF) (product gases are analyzed in Fig. S2†). As shown in Fig. 1d and e, the ordered structure of DNF-9(Fe) was observed by high resolution transmission electron microscopy (HRTEM). The acquired HRTEM image shows the visible microporous channels, with the structure in agreement with the simulated model decoded from the single crystal measurement. The zero-field Mössbauer spectrum of the sample recorded at 298 K exhibits quadrupole doublets, which could indicate the oxidation state of specific Fe centers as well as the protonation state of the atom bridge (Fig. 2a).[24] The two distinct doublets are characteristics of hyperfine parameters typical of high-spin Fe^{II} with isomer shift $\delta = 1.252$ mm s^{-1} and quadrupole splitting $|\Delta E_Q| = 2.993$ mm s^{-1}, whereas the other two can be assigned to high-spin Fe^{III} with isomer shift $\delta = 0.445$ mm s^{-1} and quadrupole splitting $|\Delta E_Q| = 0.612$ mm s^{-1}. Furthermore, it also demonstrates that $Fe^{(II\text{ or }III)}$–F species, rather than normal oxo-bridged complexes, *e.g.*, Fe–O–Fe with $\delta = 0.45$–0.52 mm s^{-1} and $|\Delta E_Q| = 1.27$–1.80 mm s^{-1} at 298 K, or hydroxo-bridged complexes, *e.g.*, Fe–OH–Fe with $\delta = 0.45$–0.52 mm s^{-1} and $|\Delta E_Q| = 0.25$–0.56 mm s^{-1} under the same conditions, that were reported before, are coordinated with iron atoms.[25] As a result, the configuration of μ-F influences the asymmetry of electron distribution, causing a large quadrupole splitting.[21,26] The presence of bridged and terminal fluorine atoms is also verified in the solid state ^{19}F Nuclear Magnetic Resonance (^{19}F-NMR) analyses (Fig. S3†).[27,28] The relative areas of the Mössbauer doublets further reveal the existence of Fe^{II} (33.31%) and Fe^{III} (66.69%), consistent with the single crystal data.

Fig. S4† shows the powder X-ray diffraction (PXRD) patterns of DNL-9(Fe), indicating good purity and crystallinity. Fig. S5† presents the argon adsorption isotherm at 87 K, which suggests a type I isotherm for a microporous structure with Brunauer–Emmett–Teller (BET) area and micropore volume being 1135 m^2 g^{-1} and 0.38 cm^3 g^{-1} for the guest-free MOF, respectively; the average pore size of the solvent-free channels is around 5.5 Å, in line with the crystallographic value from the single-crystal structure. Fig. S6 and Table S4† show that the adsorption of N_2 at 77 K gives a bit smaller BET area (1113 m^2 g^{-1}) and

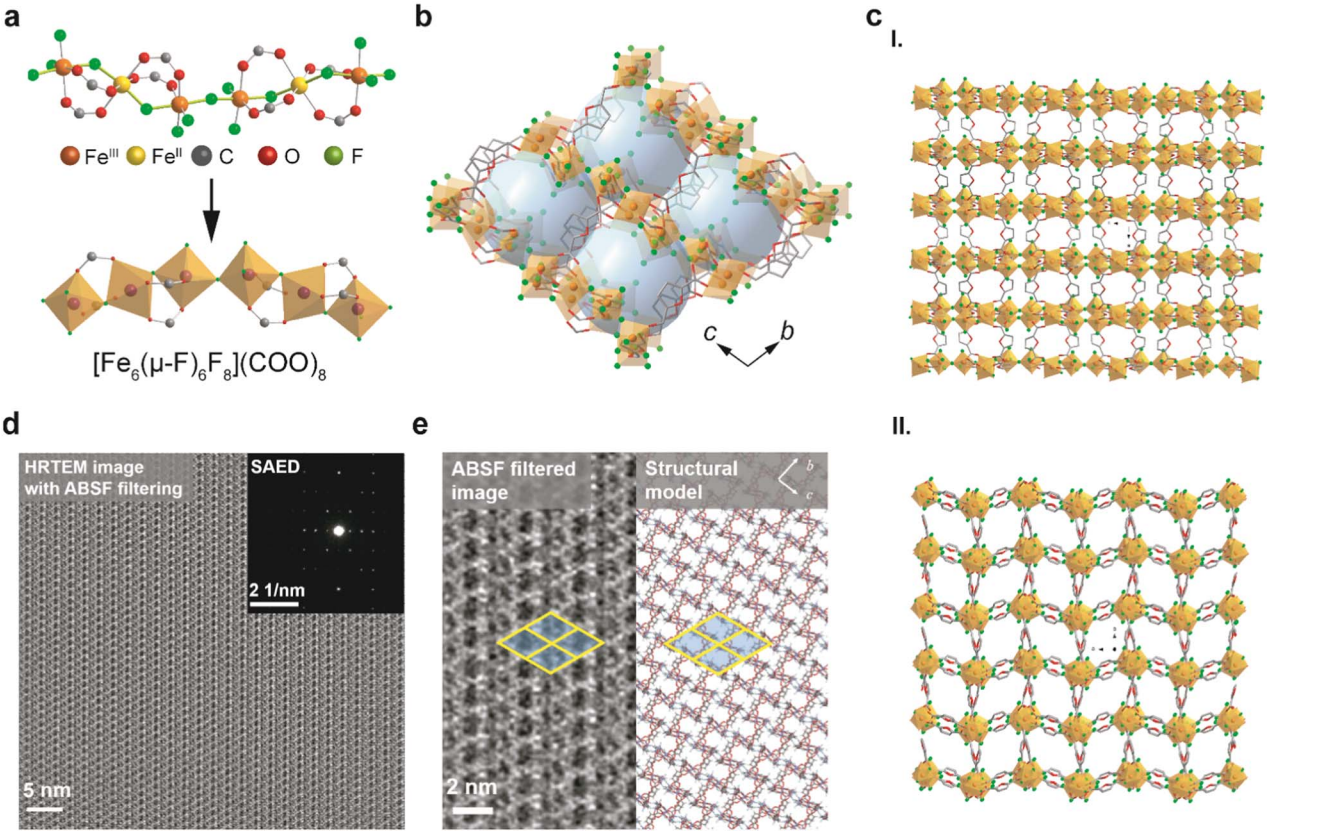

Fig. 1 (a) The structure of the fluorine coordination and the helical chain of DNL-9(Fe); (b) the framework viewed along the *a*-axis (balls indicate cavities), (c) the structure of DNL-9(Fe) viewed along the (I) *b*-axis and (II) *c*-axis; (d) low-dose motion-corrected high-resolution TEM (HRTEM) image of DNL-9(Fe) denoised by using ABSF filtering; inset: the SAED pattern. (e) Enlarged HRTEM image (left) matched with the structural model of DNL-9(Fe) viewing along the *a*-axis (right).

a slightly larger average pore size (5.8 Å) for the MOF. Thermogravimetric analysis (TGA) and differential scanning calorimetry (DSC) profiles of DNL-9(Fe) verified its decent thermal stability up to *ca.* 250 °C, with no phase transformation confirmed by structure comparisons (Fig. S7a†). The obvious weight loss in 50–200 °C in the TGA curve is due to the desorption of H_2O molecules, as evidenced by the broad peak in a similar temperature range in the mass spectra (Fig. S7b and c†). SEM images reveal the layered morphology of the samples (Fig. S8†).

Fig. 2b and S14–S16† display C_2H_2 and CO_2 single gas adsorption isotherms at 288, 298 and 308 K over 0–1 bar, which are well-fitted within the dual-site Langmuir–Freundlich (DSLF) model. In the tests, DNL-9(Fe) adsorbs far more C_2H_2 than CO_2; at 298 K and 1 bar, the adsorption capacity of C_2H_2 reaches 5.42 mol kg^{-1}, twice as much of CO_2, which is among the best results reported.[14,29,30] The adsorption enthalpies (Fig. 2b) are 26.1–28.0 kJ mol^{-1} for C_2H_2 and 25.6–26.5 kJ mol^{-1} for CO_2, both exhibiting a decrease with increasing gas loadings, indicating the presence of preferential adsorption sites in MOFs. The ideal adsorbed solution theory (IAST) selectivities were then calculated for equimolar C_2H_2/CO_2 mixtures (Fig. S17; fitting parameters: Table S6†),[31] which grow from 1.06 to 2.68 (1 bar and 288 K) with decreasing temperature and increasing pressure. This is important because, in the narrow channels of DNL-9(Fe), more adsorption of C_2H_2, either at lower temperatures or higher pressures, will prohibit the coexisting adsorption of CO_2, thus benefiting the selectivities.

Dispersion-corrected density functional theory (DFT-D3) calculations were performed to gain molecular insights into the gas adsorption behavior in DNL-9(Fe). Fig. 2c reveals the preferential binding sites for C_2H_2 and CO_2 in DNL-9(Fe), facilitated by hydrogen bonding. C_2H_2 has two such sites: the primary one is formed through $F\cdots H_{C_2H_2}$ ($F^{\delta-}$, terminal fluorine atom binding with metal; $H_{C_2H_2}{}^{\delta+}$, hydrogen atom from acetylene), with interaction distances of 2.40–2.52 Å; the other one stems from the interaction of $O_F\cdots H_{C_2H_2}$ ($O_F{}^{\delta-}$, O atom from furan rings) with distances of 2.55 Å (Fig. S20a†). The second site involves competitive adsorption, as O atoms from CO_2 ($O_{CO_2}{}^{\delta-}$) could also bind with H atoms from furan rings ($H_F{}^{\delta+}$), forming hydrogen bonding of $H_F\cdots O_{CO_2}$ with distances of 2.92–3.20 Å. In all, C_2H_2 was found to have a lower static binding energy with the framework than CO_2 (−31.78 *vs.* −28.56 kJ mol^{-1}), matching with the trend in adsorption enthalpies.

To verify the above theoretical findings in experiments, FT-IR analysis was carried out; Fig. 2d presents the spectra of blank DNL-9(Fe), and the samples adsorbed with C_2H_2, CO_2 or water. The signals observed in the curves, *e.g.*, $\nu(\equiv C\text{–}H)$ = 3226–3234

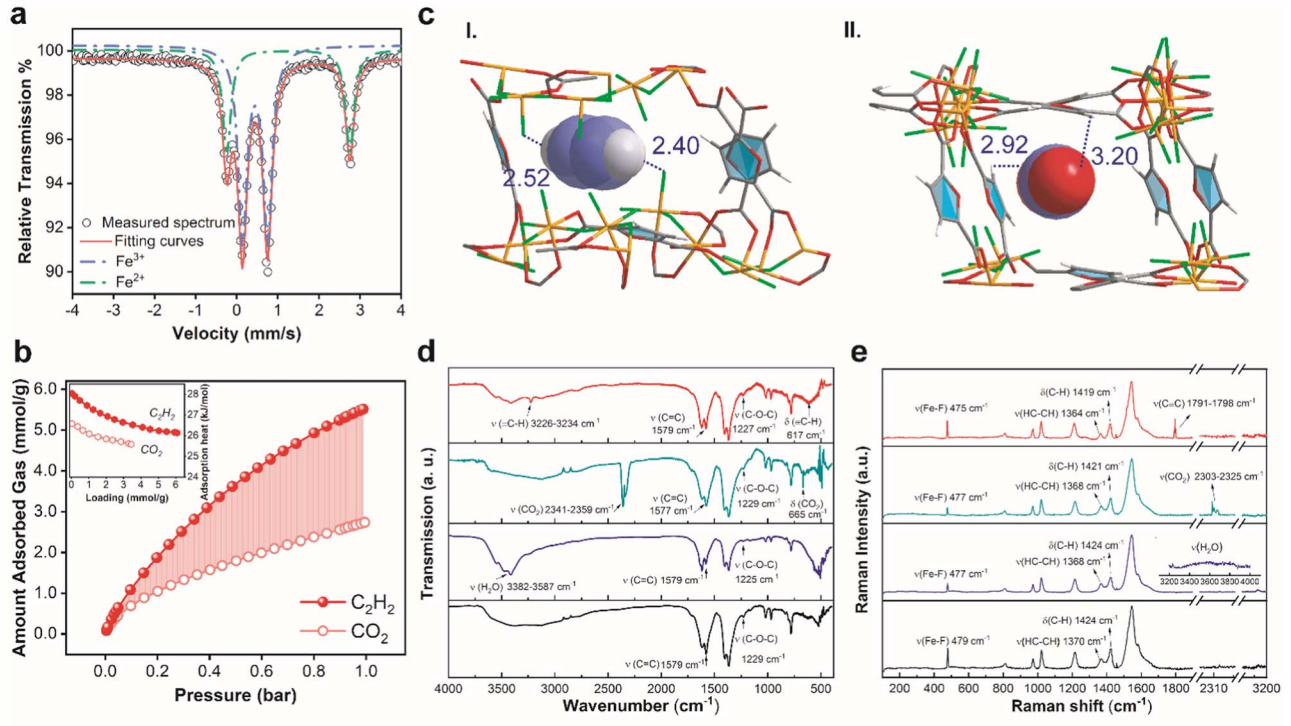

Fig. 2 (a) ^{57}Fe Mössbauer spectrum of DNL-9(Fe) at room temperature. Green and purple dash lines indicate fitted adsorption doublets assigned to Fe^{II} and Fe^{III}, respectively. The hollow circles denote the measured spectrum and the red curve represents summed fitted spectra; (b) pure gas adsorption isotherms and enthalpies (inset) of C_2H_2 and CO_2 at 298 K; (c) the adsorption status of (I) C_2H_2 and (II) CO_2 molecule in MOF *via* DFT-D3 optimization; unit: Å. Green, F; red, O; grey, C; yellow, Fe; white, H; (d) FT-IR spectra of DNL-9(Fe). Samples from bottom to top: blank MOF, H_2O-, CO_2- and C_2H_2-adsorbed (1 bar, 298 K) MOF, referenced to the KBr pellet; (e) Raman spectra of DNL-9(Fe). Samples from bottom to top: blank MOF, H_2O-, CO_2- and C_2H_2-adsorbed (1 bar, 298 K) MOF.

cm^{-1} and ν(C=O) = 2341–2359 cm^{-1},[32] prove the presence of C_2H_2 and CO_2 adsorbed in MOFs. Compared to the reference and CO_2 loaded sample, adsorption of C_2H_2 led the bands of ν(C–O–C) to shift from 1229 to 1227 cm^{-1}, driven by the interactions between furans (O_F) and C_2H_2 *via* H-bonding of $O_F\cdots H_{C_2H_2}$, as described in the above DFT findings. Raman spectra (Fig. 2e) were also recorded, where signals for the adsorption of gas molecules were clearly present. Besides, the peak seen at 479 cm^{-1} in the blank sample was attributed to the stretching of Fe–F, rather than ν(Fe–O) = 520–550 cm^{-1}, normally found in other Fe-MOFs.[32] The peak moved to lower values of 477 and 475 cm^{-1} with the adsorption of CO_2 and C_2H_2, which indicates that the fluorine regions could preferentially trap C_2H_2, possibly through the H-bonding of $F_\mu\cdots H_{C_2H_2}$ as stated above. Similar trends were also witnessed in the shifts of ν(HC–CH) and δ(C–H) bands (in furan rings), implying that C_2H_2 had superior competitive adsorption to CO_2, *via* the interactions with the ligands.

Meanwhile, Fig. 2d and e also suggest that the changes in the profiles of FT-IR and Raman were generally weaker, upon contacting the framework with water compared to C_2H_2 and CO_2. Fig. S10† shows the water sorption isotherm of DNL-9(Fe) at 298 K, where the uptake was nominal with a relative pressure <0.2. Afterwards, it increased gradually until close to saturation, with the final uptake approaching 19 wt%. We also evaluated the initial differential adsorption heat of H_2O on DNL-9(Fe) to be *ca.* 43.5 kJ mol^{-1}, which is lower than that of other FDCA-based MOFs, *e.g.*, MIL-160 (54 kJ mol^{-1}),[33] and PCN-233 (62–77 kJ mol^{-1}).[34] DFT calculations further reveal that the dominant water adsorption occurred in the cavity near the furan linker in DNL-9(Fe), with the corresponding $O_F^I\cdots H_W^I$ distance of 2.02 Å, and a $F_{\mu_2}^I\cdots H_W^{II}$ distance of 2.01 Å (Fig. S20b†). This configuration generated a binding strength of −47.5 kJ mol^{-1}, notably smaller than that of MIL-160(Al) and PCN-233 (FeNi),[34] and comparable to that of another famous fluorinated MOF, *i.e.*, FMOF-1 (−46.0 kJ mol^{-1}).[35] Importantly, we also exposed DNL-9(Fe) to water, acidic/basic (pH = 2, 10) aqueous solutions, and typical organic solvents (MeOH, EtOH, MeCN). Fig. S4 and S9† show that the structural and adsorption properties of DNL-9(Fe) almost remain the same, demonstrating the exceptional hydrochemical stability of the material.

Next, experimental breakthrough tests were carried out to examine the separation performance of DNL-9(Fe) in practical scenarios, where equimolar C_2H_2/CO_2 mixtures were passed through a homemade apparatus (Fig. S11†) with a total flow rate of 5 ml min^{-1} under dry or wet (*ca.* 90% RH) conditions at 298 K and 1 bar. An efficient separation was readily achieved in the dry atmosphere (Fig. 3a), in which CO_2 first broke the column at about 21 min, and after a long period of *ca.* 47 min, C_2H_2 came out, whilst under the humid condition, the breakthrough curves only shifted a bit to earlier moments, resulting from the competitive adsorption of water. The efficient separation of

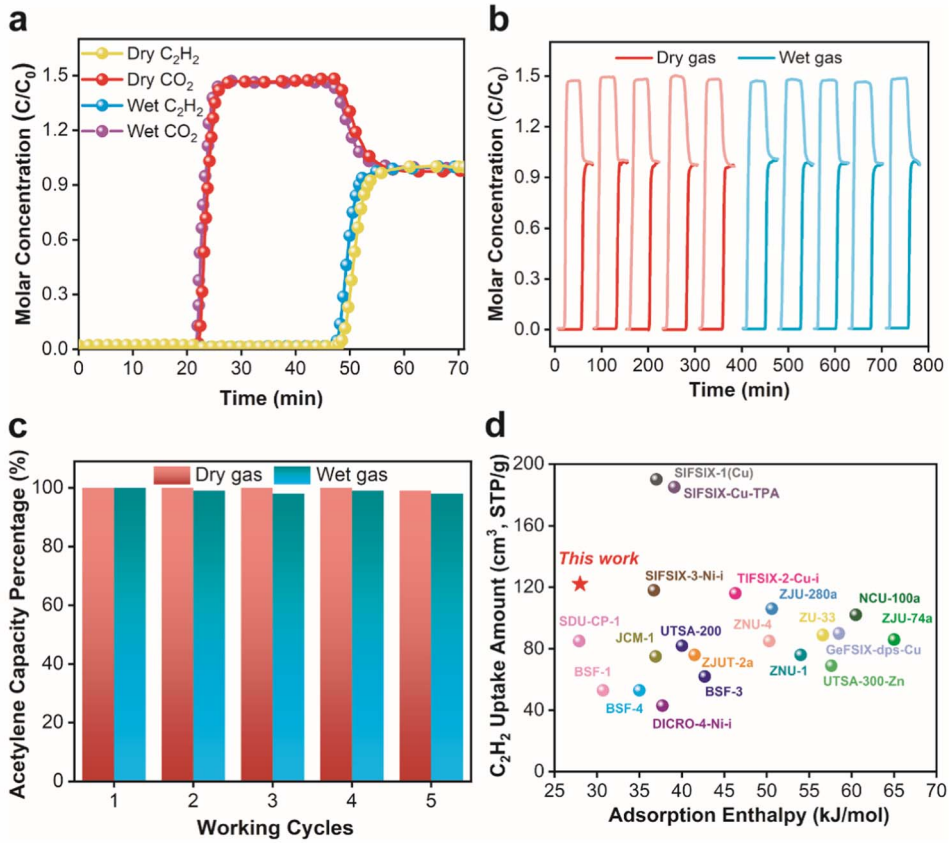

Fig. 3 (a) Experimental breakthrough curves for binary C_2H_2/CO_2 mixtures (50/50, v/v) on DNL-9(Fe) under dry and wet (*ca.* 90% RH) conditions; the cycling tests under dry and moist conditions at 298 K and 1 bar. (b) Breakthrough curves of C_2H_2 (dark) and CO_2 (light), (c) the recovery degree of C_2H_2 capacity; (d) comparison of the adsorption capacity (from static adsorption isotherms) and adsorption enthalpy of C_2H_2 for state-of-art HBA-type MOF materials. All the above: at 298 K and 1 bar.

C_2H_2/CO_2 could also be witnessed at higher temperatures under consistent conditions, albeit also with left moves of breakthrough points primarily due to lower gas uptakes at 308 K and 318 K (Fig. S13†). C_2H_2/CO_2 breakthrough selectivity was then calculated to be 2.48, which agrees with the IAST selectivities at 298 K and 1 bar. At extremely low pressures (*i.e.*, below 0.05 bar), the similar initial slopes of uptake for C_2H_2 and CO_2 also encourage us to study the adsorption kinetics for an efficient separation in DNL-9(Fe) (Fig. S18 and S19†). Table S8† shows the calculated diffusion coefficients of C_2H_2 (4.40×10^{-12} m^2 s^{-1}) and CO_2 (8.63×10^{-12} m^2 s^{-1}) under the same conditions: the much lower diffusion rate of C_2H_2 than CO_2 at 0.005 bar is due to the diffusion limitation rising from the intermolecular H-bonding interaction between C_2H_2 molecules and the framework.

Fig. 3b and c show the cycling tests for the separation under dry and wet conditions, where over 97% of C_2H_2 capacities were recovered in all cycles, when simply activating the adsorbent under a dynamic vacuum at *ca.* 0.00001 bar (0.007 Torr, absolute pressure) for 2 h at 298 K before each cycle. This is a gift from the mild gas adsorption enthalpies because of the fluorinated and saturated framework. Upon five cycles, C_2H_2 adsorption capacities were up to 3.83–3.91 mol kg^{-1}, even with the competitive adsorption of CO_2 and moisture. Again, Fig. S4 and S5† demonstrate that the MOF structure remained intact after the cycling tests either under dry conditions or even at a high relative humidity of 90%, with no obvious degradation in the structural crystallinity and surface area. Fig. 3d compares the adsorption capacity and enthalpy of C_2H_2 of DNL-9(Fe) and other state-of-art HBA-type anionic MOFs reported under the same conditions. Also with a moderate C_2H_2/CO_2 selectivity compared with other benchmark MOFs (Table S10†), DNL-9(Fe) presents a high C_2H_2 capacity, and the lowest C_2H_2 adsorption enthalpy compared to other HBA-type MOFs.[14,29,30] The latter is significant in real scenes, as it may mitigate the demands of the equipment to withstand heating, and cut down energy consumption for sorbent regeneration. Besides, Table S11† summarizes the C_2H_2/CO_2 separation performance of benchmark MOFs, including C_2H_2 static adsorption and normalized breakthrough capacity, as well as the separation time per weight of adsorbent. Clearly, DNL-9(Fe) has above-average static and normalized breakthrough capacity for C_2H_2 among all MOFs, and is superior to most HBA-containing MOFs. Overall, with the above-mentioned intriguing separation performance, as well as being prepared from cheap components (iron nodes and bio-derived massive ligands) and convenient synthesis methods,

DNL-9(Fe) is a rather promising candidate sorbent for acetylene purification in real-world applications.

Conclusions

In summary, we here reported a new fluorinated MOF, *i.e.*, DNL-9(Fe), serving as an HBA for efficient C_2H_2/CO_2 separation. This material has bridged and terminal fluorine species directly bonded with the metal. The static/dynamic adsorption tests show that the MOF displays a prominent C_2H_2/CO_2 separation performance either under dry conditions or at a high relative humidity of 90%, as well as a low adsorption enthalpy with a robust structure which is particularly beneficial for practical applications, *e.g.*, in the vacuum swing adsorption (VSA) processes. DFT calculations suggest multiple C_2H_2-favored adsorption sites with MOF–C_2H_2 hydrogen-bonding interactions in DNL-9(Fe), which is further proved by the FT-IR and Raman measurements. All results manifest that DNL-9(Fe) is very promising to be utilized as a sorbent for acetylene purification in industry.

Data availability

All experimental supporting data and procedures are available in the ESI.†

Author contributions

Y.-M. G., Y.-Y. Y. and C.-L. C. contributed equally to this work. Conceptualization: Y.-M. G., X.-W. L. and S.-D. W. Methodology: Y.-M. G. and X.-W. L. Investigation: Y.-M. G., Y.-Y. Y., C.-L. C., S.-S. Z., T.-J. S. and Y. H. Validation: X.-W. L., Z. L. and S.-D. W. Visualization: Y.-M. G, Y.-Y. Y. and C.-L. C. Writing – original draft: Y.-M. G. and X.-W. L. Writing – review & editing: X.-W. L., Z. L. and S.-D. W. Supervision: X.-W. L., Z. L. and S.-D. W.

Conflicts of interest

The authors declare that they have no competing interests.

Acknowledgements

Y.-M. G., T.-J. S. and S.-D. W. are grateful to the National Natural Science Foundation of China for funding (No. 21776266). X.-W. L. and Z. L. appreciate the funding (BAS/1/1375-01-01 and FCC/1/1972-88-01) from King Abdullah University of Science and Technology (KAUST). The authors also thank Prof. Alexandre Rykov at the Center for Advanced Mössbauer Spectroscopy in DICP, for Mössbauer spectroscopy measurement and analysis; and Dr Wen-Guang Yu and Dr Pei-Fang Yan for the help in TGA-DSC and IGA adsorption measurements.

Notes and references

1 Y. Ye, S. Xian, H. Cui, K. Tan, L. Gong, B. Liang, T. Pham, H. Pandey, R. Krishna, P. C. Lan, K. A. Forrest, B. Space, T. Thonhauser, J. Li and S. Ma, *J. Am. Chem. Soc.*, 2022, **144**, 1681–1689, DOI: **10.1039/d2qi01989b**.

2 P. Pässler, W. Hefner, K. Buckl, H. Meinass, A. Meiswinkel, H.-J. Wernicke, G. Ebersberg, R. Müller, J. Bässler, H. Behringer and D. Mayer, in *Ullmann's Encyclopedia of Industrial Chemistry*, 2011, DOI: **10.1002/14356007.a01_097.pub4**.

3 J. Liu, J. W. Lam and B. Z. Tang, *Chem. Rev.*, 2009, **109**, 5799–5867, DOI: **10.1021/cr900149d**.

4 V. I. Savchenko, A. V. Nikitin, I. V. Sedov, A. V. Ozerskii and V. S. Arutyunov, *Chem. Eng. Sci.*, 2019, **207**, 744–751, DOI: **10.1016/j.ces.2019.07.012**.

5 J. R. Li, R. J. Kuppler and H. C. Zhou, *Chem. Soc. Rev.*, 2009, **38**, 1477–1504, DOI: **10.1039/B802426J**.

6 Y.-M. Gu, H.-F. Qi, T.-T. Sun, X.-W. Liu, S. Qadir, T.-J. Sun, D.-F. Li, S.-S. Zhao, D. Fairen-Jimenez and S.-D. Wang, *Chem. Mater.*, 2022, **34**, 2708–2716, DOI: **10.1021/acs.chemmater.1c04168**.

7 B. Wang, L. H. Xie, X. Q. Wang, X. M. Liu, J. P. Li and J. R. Li, *Green Energy Environ.*, 2018, **3**, 191–228, DOI: **10.1016/j.gee.2018.03.001**.

8 L. Yang, S. Qian, X. Wang, X. Cui, B. Chen and H. Xing, *Chem. Soc. Rev.*, 2020, **49**, 5359–5406, DOI: **10.1039/C9CS00756C**.

9 Z. J. Zhang, S. C. Xiang and B. L. Chen, *CrystEngComm*, 2011, **13**, 5983–5992, DOI: **10.1039/C1CE05437F**.

10 N. Xu, J. B. Hu, L. Y. Wang, D. Luo, W. Q. Sun, Y. Q. Hu, D. M. Wang, X. L. Cui, H. B. Xing and Y. B. Zhang, *Chem. Eng. J.*, 2022, **450**, 138034, DOI: **10.1016/j.cej.2022.138034**.

11 P. Z. Moghadam, A. Li, X. W. Liu, R. Bueno-Perez, S. D. Wang, S. B. Wiggin, P. A. Wood and D. Fairen-Jimenez, *Chem. Sci.*, 2020, **11**, 8373–8387, DOI: **10.1039/d0sc01297a**.

12 M. Ding, R. W. Flaig, H. L. Jiang and O. M. Yaghi, *Chem. Soc. Rev.*, 2019, **48**, 2783–2828, DOI: **10.1039/C8CS00829A**.

13 A. Cadiau, Y. Belmabkhout, K. Adil, P. M. Bhatt, R. S. Pillai, A. Shkurenko, C. Martineau-Corcos, G. Maurin and M. Eddaoudi, *Science*, 2017, **356**, 731–735, DOI: **10.1126/science.aam8310**.

14 H. Li, C. Liu, C. Chen, Z. Di, D. Yuan, J. Pang, W. Wei, M. Wu and M. Hong, *Angew. Chem., Int. Ed.*, 2021, **60**, 7547–7552, DOI: **10.1002/anie.202013988**.

15 J. Wang, Y. Zhang, Y. Su, X. Liu, P. Zhang, R. B. Lin, S. Chen, Q. Deng, Z. Zeng, S. Deng and B. Chen, *Nat. Commun.*, 2022, **13**, 200, DOI: **10.1038/s41467-021-27929-7**.

16 J. Wang, Y. Zhang, P. Zhang, J. Hu, R. B. Lin, Q. Deng, Z. Zeng, H. Xing, S. Deng and B. Chen, *J. Am. Chem. Soc.*, 2020, **142**, 9744–9751, DOI: **10.1021/jacs.0c02594**.

17 C. Yang, X. Wang and M. A. Omary, *J. Am. Chem. Soc.*, 2007, **129**, 15454–15455, DOI: **10.1021/ja0775265**.

18 C. A. Fernandez, J. Liu, P. K. Thallapally and D. M. Strachan, *J. Am. Chem. Soc.*, 2012, **134**, 9046–9049, DOI: **10.1021/ja302071t**.

19 T. H. Chen, I. Popov, W. Kaveevivitchai, Y. C. Chuang, Y. S. Chen, A. J. Jacobson and O. S. Miljanic, *Angew. Chem., Int. Ed.*, 2015, **54**, 13902–13906, DOI: **10.1002/anie.201505149**.

20 Z. Shi, Y. Tao, J. Wu, C. Zhang, H. He, L. Long, Y. Lee, T. Li and Y. B. Zhang, *J. Am. Chem. Soc.*, 2020, **142**, 2750–2754, DOI: **10.1021/jacs.9b12879**.

21 S. Dammers, T. P. Zimmermann, S. Walleck, A. Stammler, H. Bogge, E. Bill and T. Glaser, *Inorg. Chem.*, 2017, **56**, 1779–1782, DOI: **10.1021/acs.inorgchem.6b03093**.

22 A. Ebadi Amooghin, H. Sanaeepur, R. Luque, H. Garcia and B. Chen, *Chem. Soc. Rev.*, 2022, **51**, 7427–7508, DOI: **10.1039/D2CS00442A**.

23 W. J. Shi, Y. Z. Li, J. Chen, R. H. Su, L. Hou, Y. Y. Wang and Z. Zhu, *Chem. Commun.*, 2021, **57**, 12788–12791, DOI: **10.1039/D1CC05196B**.

24 J. L. Lee, S. Biswas, C. Sun, J. W. Ziller, M. P. Hendrich and A. S. Borovik, *J. Am. Chem. Soc.*, 2022, **144**, 4559–4571, DOI: **10.1021/jacs.1c12888**.

25 D. M. Kurtz, *Chem. Rev.*, 2002, **90**, 585–606, DOI: **10.1021/cr00102a002**.

26 U. Bossek, H. Hummel, T. Weyhermüller, E. Bili and K. Wieghardt, *Angew. Chem., Int. Ed.*, 1996, **34**, 2642–2645, DOI: **10.1002/anie.199526421**.

27 J. M. Miller, *Prog. Nucl. Magn. Reson. Spectrosc.*, 1996, **28**, 255–281, DOI: **10.1016/0079-6565(95)01024-6**.

28 N. Bouzidia, B. Hamdi and A. Ben Salah, *Chem. Res. Chin. Univ.*, 2016, **32**, 519–526, DOI: **10.1007/s40242-016-6012-y**.

29 K. J. Chen, H. S. Scott, D. G. Madden, T. Pham, A. Kumar, A. Bajpai, M. Lusi, K. A. Forrest, B. Space, J. J. Perry and M. J. Zaworotko, *Chem*, 2016, **1**, 753–765, DOI: **10.1016/j.chempr.2016.10.009**.

30 Q. L. Qian, X. W. Gu, J. Y. Pei, H. M. Wen, H. Wu, W. Zhou, B. Li and G. D. Qian, *J. Mater. Chem. A*, 2021, **9**, 9248–9255, DOI: **10.1039/D0TA11340A**.

31 A. L. Myers and J. M. Prausnitz, *AIChE J.*, 1965, **11**, 121–127, DOI: **10.1002/aic.690110125**.

32 K. I. Hadjiivanov, D. A. Panayotov, M. Y. Mihaylov, E. Z. Ivanova, K. K. Chakarova, S. M. Andonova and N. L. Drenchev, *Chem. Rev.*, 2021, **121**, 1286–1424, DOI: **10.1021/acs.chemrev.0c00487**.

33 A. Cadiau, J. S. Lee, D. Damasceno Borges, P. Fabry, T. Devic, M. T. Wharmby, C. Martineau, D. Foucher, F. Taulelle, C. H. Jun, Y. K. Hwang, N. Stock, M. F. De Lange, F. Kapteijn, J. Gascon, G. Maurin, J. S. Chang and C. Serre, *Adv. Mater.*, 2015, **27**, 4775–4780, DOI: **10.1002/adma.201502418**.

34 Y.-M. Gu, H.-F. Qi, S. Qadir, X.-W. Liu, T.-J. Sun, S.-S. Zhao, Z. Lai and S.-D. Wang, *ACS Sustainable Chem. Eng.*, 2021, **9**, 17310–17318, DOI: **10.1021/acssuschemeng.1c06207**.

35 K. Tan, N. Nijem, Y. Gao, S. Zuluaga, J. Li, T. Thonhauser and Y. J. Chabal, *CrystEngComm*, 2015, **17**, 247–260, DOI: **10.1039/C4CE01406E**.